APPLIED SCIENCES AND ENGINEERING

Fine structural tuning of the assembly of ECM peptide conjugates via slight sequence modifications

Jingya Qin¹, Jennifer D. Sloppy¹, Kristi L. Kiick^{1,2}*

The self-assembly of nanostructures from conjugates of elastin-like peptides and collagen-like peptides (ELP-CLP) has been studied as means to produce thermoresponsive, collagen-binding drug delivery vehicles. Motivated by our previous work in which ELP-CLP conjugates successfully self-assembled into vesicles and platelet-like nanostructures, here, we extend our library of ELP-CLP bioconjugates to a series of tryptophan/phenylalanine-containing ELPs and GPO-based CLPs $[W_2F_x-b-(GPO)_y]$ with various domain lengths to determine the impact of these modifications on the thermoresponsiveness and morphology. The lower transition temperature of the conjugates with longer ELP or CLP domains enables the formation of well-defined nanoparticles near physiological temperature. Moreover, the morphological transition from vesicles to platelet-like nanostructures occurred when the ratio of the lengths of ELP/CLP decreased. Given the previously demonstrated ability of many ELP-CLP bioconjugates to bind to both hydrophobic drugs and collagen-containing materials, our results suggest new opportunities for designing specific thermoresponsive nanostructures for targeted biological applications.

Copyright © 2020 The Authors, some rights reserved; exclusive licensee American Association for the Advancement of Science. No claim to original U.S. Government Works. Distributed under a Creative Commons Attribution NonCommercial License 4.0 (CC BY-NC).

INTRODUCTION

Over the past few decades, the self-assembly of amphiphilic molecules has proven to be a valuable strategy for assembling smart drug delivery vehicles and tissue engineering substrates (1), with peptidebased conjugates being particularly useful owing to their tunable secondary structures, self-association, biodegradability, and biocompatibility (2). The chemical structure, molecular geometry, and solvent conditions can be tuned to affect the size, shape, and interfacial curvature of peptide-containing assembled structures (1, 2), and the development of systematic design rules for the manipulation of architectures via small changes in sequence would offer substantial opportunities to expand their use (2, 3). Stimuli-responsive domains have been incorporated that can undergo substantial property changes in response to small external changes in their environment, with triggers such as temperature, pH, and solvent (1, 3); thermoresponsiveness is perhaps the most widely used owing to its ease of application (4), and the fact that peptide conformations such as helix, β turn, and coiled-coils can be manipulated by temperature (2). Accordingly, stimuli-responsive peptide-amphiphilic copolymers have demonstrated significant promise as drug carriers (4, 5).

An important class of molecules developed for these applications is the elastin-like (poly)peptides (ELPs), which mimic features of the mammalian protein elastin, are composed largely of Val-Pro-Gly-Xaa-Gly amino acid repeat units (in which Xaa is any residue except proline) and exhibit the widely exploited lower-critical solution temperature (6) in which they are soluble in water below their transition temperature (T_1) but will collapse into a coacervate phase above that temperature (T_1). ELPs have thus been enormously versatile as smart hydrophobic domains in thermally responsive peptide amphiphilic copolymers and in peptide conjugates (8) and have been investigated for manipulating T_1 in drug delivery systems and also for targeting cells via thermally responsive mechanisms (6, 8). However, short synthetic ELPs with high inverse T_1 have been rarely studied as smart biomaterials for biological application (9), despite

the versatility they would afford, largely because at low molecular-weights, the ELPs are fully soluble under physiologically relevant conditions and do not mediate assembly. Expansion of the use of short ELPs would open important opportunities to not only explore molecular details of the lower critical solution temperature (LCST)–like transition of these molecules but also new possibilities for making amphiphiles with tailored shapes, hydrophobicity, and tissue-targeting capabilities.

As for the hydrophilic building block in stimuli-responsive peptide-based amphiphiles, short synthetic collagen-like peptides (CLPs), which adopt triple helix conformations, also have been widely studied given the thermoresponsiveness of the conformational transition (10–14) and the prevalence of collagen remodeling in the extracellular matrix under both homeostatic and pathological conditions (15). Many studies have demonstrated that unfolded CLPs can target native collagens or collagen substrates via the formation of triple helix (16, 17), and that short CLPs can be used to form and modify hydrogels, liposomes, and other structures (18–20). Despite their prevalence in these types of investigations, however, they have not been used as a design element to affect LCST-like transitions and assembled morphologies; this application of CLPs should be very fruitful given their hydrophilicity, rod-like triple-helical structure and ability to integrate in collagen-containing matrices.

In our previous work, we conjugated short synthetic ELPs (peptides, rather than polypeptides) with short synthetic triple-helical CLP domains and have shown that the association of the CLP triple helix substantially lowers the high inverse $T_{\rm t}$ of the short peptide-based ELP domain into experimentally tractable and, in some cases, physiologically relevant temperature ranges (21, 22). Subsequently, we demonstrated the formation of assembled ELP-CLP conjugates by tuning the hydrophobicity of ELP domains comprising (VPGXG)₄, in which the number of repeats equipped with phenylalanine (F) or tryptophan (W) residues in the X position was varied (23). In contrast to vesicle structures, these W-containing ELP-CLP conjugates formed nanoscale platelet morphologies under aqueous conditions. Both vesicular and platelet-like nanostructures (24) offer significant opportunities in drug delivery systems owing to the shape-dependent influence on retention and cell uptake, and

¹Department of Materials Science and Engineering, University of Delaware, Newark, DE 19716, USA. ²Delaware Biotechnology Institute, Newark, DE 19711, USA. *Corresponding author. Email: kiick@udel.edu

CLP-modified structures should be similarly useful with the added benefit of targeting to select collagens. Meanwhile, self-assembled peptide-based soft biomaterials remain attractive in biomedical applications due to their biocompatibility and ease of "bottom-up" fabrication (25, 26).

Given the great flexibility of peptides as building blocks and the demonstrated assembly of select ELP-CLP conjugates, we expected that the thermal T_t and morphologies of ELP-CLP conjugates could be sensitively manipulated by making slight changes in the hydrophobicity and length of the ELP and CLP domains. We produced a library of peptide domains comprising a series of tryptophan/ phenylalanine-containing ELPs and glycine-proline-hydroxyproline (GPO)-based CLPs with various domain lengths. Electrospray ionization mass spectrometry (ESI-MS) and high-performance liquid chromatography (HPLC) were used to confirm the purity of ELP-CLP conjugates, and the conformational and self-assembly behavior was characterized via circular dichroism (CD) spectroscopy, dynamic light scattering (DLS), transmission electron microscopy (TEM), and atomic force microscopy (AFM). Our studies clearly demonstrate the ability to tune the transitions and morphologies of these dually responsive conjugates, with a level of precision over the domain compositions and ratio of domain lengths in the ELP-CLP conjugates largely not possible in other polymer-based and/or peptidecontaining conjugates.

RESULTS

We have previously reported a select set of ELP-CLP conjugates that can self-assemble into either thermoresponsive vesicular (21, 22) or nonthermoresponsive platelet-like nanostructures (23). The formation of these structures is mediated by the thermally mediated phase separation of the ELP domain in the center of a bilayer-like structure, with triple-helical CLP domains at the surfaces of the bilayer. While conjugates comprising a (VPGFG)₆ domain chemically attached to the N-terminal end of CLP domains of different lengths and compositions uniformly adopted thermoresponsive vesicular structures, a set of (VPGXG)₄-(GPO)₈ bioconjugates (with X comprising W or F) were demonstrated to assemble into bilayer, plateletlike morphologies, although lacked thermoresponsiveness (23, 27). On the basis of these results, we sought to establish that the fine level of control in the compositions and lengths of these peptidebased, thermally triggered amphiphiles would serve as a sensitive handle for generating collagen-binding nanostructures with different morphologies and thermal responsiveness. On the basis of previous literature showing the impact of hydrophobic/hydrophilic ratios on the morphologies and sizes of self-assembled amphiphiles, we anticipated that this control would be possible, with the innovations that the transitions should be triggered with only small changes in peptide composition and length and that the assembly could be triggered by slight changes in temperatures relevant for clinical therapies.

Twelve W₂F_x-b-(GPO)_y conjugates were produced via copper(I)-mediated azide-alkyne cycloaddition reactions in which ELP variants include W₂F, W₂F₂, W₂F₃, and W₂F₄ were conjugated with CLP domains comprising (GPO)₆GG, (GPO)₈GG, or (GPO)₁₀GG sequences. C-terminally alkyne-functionalized ELP domains and N-terminally azide-functionalized CLP domains were synthesized via solid-phase peptide synthesis (SPPS) methods and purified via reverse-phase HPLC. Then, ELPs were conjugated to the CLPs via

copper(I)-catalyzed azide-alkyne cycloaddition at 90°C for 4 hours (scheme S1) (28). All bioconjugates were purified via HPLC with column heating above their CLP triple-helix unfolding temperature to avoid triple helix formation on the column. Analytical HPLC and ESI-MS were used to verify the purity and expected composition of the peptides and ELP-CLP conjugates (figs. S1 and S2).

Conformational behavior of ELP-CLP conjugates

The triple helix conformation adopted by the CLP domain in the ELP-CLP conjugates was confirmed via CD spectroscopy. The full-wavelength scan from 200 to 250 nm for the different W_2F_4 -CLP conjugates is presented in fig. S3. The clear maximum at 225 nm indicated that the CLP domains are capable of forming triple helix after conjugation with any of the studied ELP domains. The unfolding behavior of the triple helix was detected with the reduction of the intensity of the band at ca. 225 nm upon heating. The first derivative of the melting curve (red curve) suggested the melting temperature ($T_{\rm m}$) for each ELP-CLP conjugate. The CD data for the CLP triple helix formation for the different conjugates show no significant changes in the mean residue ellipticity between ELP-CLPs in which the ELP domain changes in length while the CLP domain remains constant, suggesting that this slight change in molarity does not significantly affect the triple helical stability of the conjugates (fig. S3).

The features of these spectra are completely consistent with those reported for triple-helical structures of a variety of different CLPs, indicating that these ELP-CLP conjugates adopted a triple helical conformation under the conditions reported here. Compared with the W_2F_4 -(GPO)₆GG conjugate (T_m of 64.7°C) and W_2F_4 -(GPO)₈GG conjugate ($T_{\rm m}$ of 65.1°C), to the W₂F₄-(GPO)₁₀GG conjugate exhibited a slightly higher T_m of 66.5°C, indicating that longer CLP domain presented a more stable triple helix structure. For ELP-(GPO)6GG conjugates and ELP-(GPO)₈GG conjugates (shown in table S1), the collapsed ELP domains anchor the CLP domain and stabilize it against unfolding, as the T_m values of these conjugates were higher than that of isolated CLP domains (shown in table S1 and fig. S3). However, for longer CLP-based conjugates, the $T_{\rm m}$ of ELP-(GPO)₁₀GG conjugates (shown in table S1) is slightly lower than that of isolated (GPO)₁₀GG, indicating the decreased stability of the CLP domain against unfolding, which may be a result of the morphology observed for these conjugates (see below). Furthermore, the responsiveness of the shorter CLP domains may be more substantially affected by the hydrophobicity of ELP domains due to the CLP's lower triple helical stability. For instance, the $T_{\rm m}$ of the four ELP-(GPO)₆GG conjugates shows a steady and significant increase in T_m with an increase in ELP hydrophobicity, which is more pronounced than those observed for the (GPO)₈- and (GPO)₁₀based conjugates.

Temperature responsiveness of ELP-CLP assembly

DLS studies were conducted to characterize the temperature sensitivity of assembly and the resulting diameters of assembled ELP-CLP bioconjugates. The hydrodynamic diameter (D_h) of the nanostructures was plotted as function of temperature upon heating at temperatures ranging from 4° to 80°C (Fig. 1). ELP domains alone (not conjugated to CLP) show D_h below 10 nm for the entire temperature range of the experiment, indicating that no assembly occurred and that the ELP domains are soluble over the full temperature range investigated (Fig. 1A). For the 12 ELP-CLP conjugates (Fig. 1, B to D), only the D_h of the W_2F -(GPO)₆GG conjugate (Fig. 1B, red

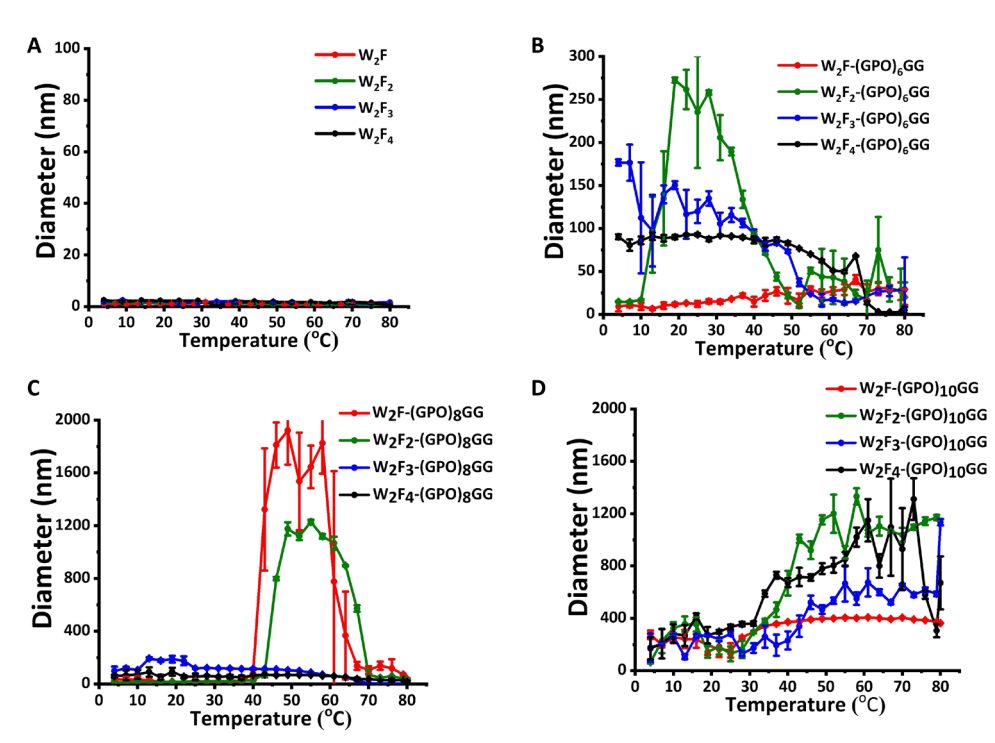


Fig. 1. Hydrodynamic diameters of nanostructures as a function of temperature upon heating. (A) ELP domains with sequence W_2F , W_2F_3 , and W_2F_4 . (B) Each ELP-(GPO)₆GG conjugate. (C) Each ELP-(GPO)₈GG conjugate. (D) Each ELP-(GPO)₁₀GG conjugate. All samples were dissolved in deionized water with concentration of 1 mg/ml.

curve) remained below 20 nm over the entire temperature range, suggesting a lack of assembly. However, the other 11 ELP-CLP conjugates are shown to assemble into nanostructures with various D_h , at temperatures that exceed the T_t of the ELP domain in the ELP-CLP conjugate, consistent with our previous reports. We note the initially large diameter of the ELP-(GPO)₁₀GG bioconjugates that suggests a T_t that is below 4°C; the observed transition at ca. 30° to 40°C (Fig. 1D) arises as a result of the aggregation of the nanoparticles (and not a T_t -mediated assembly), so the DLS measurements indicate a correspondingly larger size, which is also consistent with our TEM data (below and fig. S4). This aggregation is likely a result of possible interaggregate association of the longer (GPO)₁₀-based sequences. The subsequent rapid reduction in diameters observed for several of the conjugates with further increases in temperature (Fig. 1, B and C), results from the unfolding of the CLP domain at its $T_{\rm m}$, which then results in the resolubilization of the monomeric conjugate. The temperature at which this transition occurs generally increases with the length of the ELP (for a given CLP) owing to the increased stability of the ELP coacervate and also generally increases as the CLP length increases. Because $T_{\rm m}$ denotes the midpoint of the unfolding transition, diameters indicative of assembly can be observed for the ELP-CLP conjugates at temperatures slightly above the reported $T_{\rm m}$ [e.g., for the -(GPO)₆GG and -(GPO)₈GG conjugates; the -(GPO)₁₀GG conjugates aggregate at elevated temperatures, and thus dissociation at $T_{\rm m}$ is not observed].

Table 1 illustrates the $T_{\rm t}$ (from DLS) and $T_{\rm m}$ (from CD) values for each of the ELP-CLP conjugates. The addition of a greater number of VPGFG repeats in the W_2F_x domains significantly reduces the $T_{\rm t}$ of the conjugates due to the greater hydrophobicity of the longer, F-containing ELP domains (29). For example, the $T_{\rm t}$ of the W_2F_2 -(GPO)₆GG conjugate is 17°C, which is lowered by more than

60°C compared to the T_t of the W₂F-(GPO)₆GG (which exceeds 80°C). The T_t of the W₂F₃-(GPO)₆GG and W₂F₄-(GPO)₆GG conjugates, with longer ELP domains, is lower than 4°C, which is also consistent with the lower T_t expected for hydrophobic ELPs of increasing length. Thus, the T_t of the W_2F_2 -(GPO)₈GG conjugate, with its longer ELP domain, would be expected to be lower than that of the W₂F-(GPO)₈GG (42°C); it is actually similar/slightly higher (45°C), which, given the very similar peptide (and ELP) concentrations in the two samples (see above), most likely arises from the platelet-like morphology that is observed for these two conjugates (see below) (30). The ultimate solubility of the platelets is likely higher given the greater solvent exposure of the hydrophilic CLP bilayer surfaces, which would support a higher T_t that may be less sensitive to the length of the ELP domain. The remaining ELP-(GPO)₈GG conjugates show the expected reduction in T_t with increasing ELP length with T_t values of less than 4°C for the W_2F_3 -(GPO)₈GG and W_2F_4 -(GPO)₈GG.

An increase in the length of the CLP domain also generally results in a reduction in the $T_{\rm t}$ of the ELP-CLP conjugates, despite the hydrophilicity of the CLP domain (which would be expected to cause an increase in the $T_{\rm t}$ as the CLP becomes longer). For example, the $T_{\rm t}$ of W₂F-(GPO)₆GG is higher than 80°C, while the $T_{\rm t}$ values of W₂F-(GPO)₈GG and W₂F-(GPO)₁₀GG are 42°C and below 4°C, respectively. This likely results from the increased stability of the longer CLP domains, which would be expected to increase the local concentration of the ELP domains to a greater extent and cause the reduction of the observed $T_{\rm t}$. A notable exception to this trend is the W₂F₂-(GPO)₈GG conjugate, which, by this reasoning, would be expected to exhibit a lower $T_{\rm t}$ than that of the W₂F₂-(GPO)₆GG (17°C), rather than the observed value of 45°C. As described above, this significant deviation from expectation is likely

ELP-CLP conjugate	T _t (°C)	T _m (°C)	Ratio of ELP/CLP length	Morphology	Diameter (μm)	Thickness (nm
W ₂ F(GPO) ₆ GG	>80	33.1	0.6	N/A	N/A	N/A
W ₂ F ₂ (GPO) ₆ GG	17	33.1	0.66	Vesicle	0.25	13.7
W ₂ F ₃ -(GPO) ₆ GG	<4	49.1	0.71	Vesicle	0.15	12.5
W ₂ F ₄ -(GPO) ₆ GG	<4	64.7	0.75	Vesicle	0.09	12.9
W ₂ F-(GPO) ₈ GG	42	64.1	0.46	Platelet	0.5 × 1.0	20.4
W ₂ F ₂ -(GPO) ₈ GG	45	57.2	0.51	Platelet	0.6 × 1.0	20.3
W ₂ F ₃ -(GPO) ₈ GG	<4	64.1	0.54	Vesicle	0.12	14.4
W ₂ F ₄ -(GPO) ₈ GG	<4	65.1	0.58	Vesicle	0.08	16.3
W ₂ F-(GPO) ₁₀ GG	<4	67.4	0.37	Platelet	0.5 × 0.6	21.3
W ₂ F ₂ -(GPO) ₁₀ GG	<4	68.3	0.41	Platelet	0.4 × 0.6	21.9
W ₂ F ₃ -(GPO) ₁₀ GG	<4	67.7	0.44	Platelet	0.4 × 0.6	21.8
W ₂ F ₄ -(GPO) ₁₀ GG	<4	66.5	0.47	Platelet	0.4 × 0.6	22.6

related to the platelet-like morphology of the W_2F_2 -(GPO)₈GG, which may have more favorable interactions with water than the vesicles formed by W_2F_2 -(GPO)₆GG, resulting in a substantially increased T_t . All (GPO)₁₀GG conjugates, regardless of the composition of the ELP domain, however, exhibit T_t values below 4°C because of the longer length and stability of the CLP domain.

In addition, the dimensions of the various nanostructures differ significantly with the identity of the specific ELP-CLP conjugate. As shown in Fig. 1 (B and C) and delineated in Table 1, ELP-CLP conjugates forming spherical structures exhibited $D_{\rm h}$ values of approximately 80 to 250 nm, at temperatures above the $T_{\rm t}$. In contrast, ELP-CLP conjugates, which self-assembled into platelets (confirmed via TEM, see below), show larger apparent $D_{\rm h}$ values of approximately 1000 nm (but no significant precipitation). The nanostructures began to dissociate at temperatures above the CD-determined $T_{\rm m}$ of the CLP domain [with the exception of the -(GPO)₁₀GG conjugates, which aggregated at elevated temperatures].

The dual-temperature responsiveness of the assembly of these structures is illustrated in Fig. 2. Soluble ELP-CLP diblock trimers can self-assemble into nanostructures (vesicles or platelets) when the temperature is increased above the $T_{\rm b}$ but remains below the $T_{\rm m}$, of an ELP-CLP conjugate; the collapsed ELP domain is sequestered in a bilayer structure between the relatively hydrophilic, folded CLP domains on the surfaces. With an increase in temperature above the $T_{\rm m}$ of a given conjugate, these nanostructures dissociate into ELP-CLP conjugate monomers, which are soluble in aqueous solution and thus yield significantly reduced $D_{\rm h}$ values similar to those of the soluble trimer. Some ELP-CLP conjugates exhibit thermoresponsive transitions in clinically relevant ranges [e.g., W_2F_2 -(GPO)₆GG with $T_{\rm t}$ value of 17°C and $T_{\rm m}$ value of 33°C], which might be useful in biological applications for drug delivery under hypothermic conditions.

Morphological features of ELP-CLP conjugates

TEM and cryogenic TEM (cryo-TEM) were conducted to investigate the morphology of the nanostructures self-assembled from the ELP-CLP conjugates at various temperatures. With the exception of the W₂F-(GPO)₆GG conjugate, which does not assemble at any temperature below 80°C, all other ELP-(GPO)₆GG conjugates self-

assembled into structures with diameters/dimensions ranging from 80 to 250 nm (fig. S4A), which is consistent with the DLS data (Fig. 1). Figure 3 shows the morphology of the ELP-(GPO)₈GG conjugates, which form platelet-like nanostructures for the conjugates with shorter ELP domains, with a transformation to spherical nanostructures with an increase in length of the ELP domain. The ELP-(GPO)₈GG conjugates with longer ELP domains (higher ELP/ CLP ratio) (W₂F₃-(GPO)₈GG and W₂F₄-(GPO)₈GG) self-assembled into spherical nanostructures (Fig. 3, C and D), at select temperatures, similar to those formed by the ELP-(GPO)₆GG conjugates (fig. S4A). In contrast, nonspherical, platelet-like nanostructures were detected when the ELP/CLP ratio decreased, as illustrated in the TEM images for the W₂F-(GPO)₈GG and W₂F₂-(GPO)₈GG conjugates (Fig. 3, A and B); the use of the term "platelet-like" refers only to the shape of these structures. In contrast to the thermal nonresponsiveness of the nanoplatelets we have reported in our previous work, these two ELP-CLP conjugates self-assembled into thermoresponsive nanoplatelets, which could expand their versatility in delivery applications. The entire series of ELP-(GPO)₁₀GG conjugates formed platelets, all with apparent T_t values lower than 4°C (fig. S4B).

Cryo-TEM was conducted to further determine the vesicular structure and thickness of the nanoparticles from ELP-CLP conjugates incubated at 37°C. The spherical nanostructures observed in the cryo-TEM clearly are confirmed to be vesicular in nature (Fig. 4 and fig. S5), with spherical structures formed by a bilayer. The vesicles for W₂F₂-(GPO)₆GG, W₂F₃-(GPO)₆GG, W₂F₄-(GPO)₆GG, W₂F₃-(GPO)₈GG, and W₂F₄-(GPO)₈GG were indicated to have diameters of approximately 250 \pm 18, 150 \pm 8, 90 \pm 7, 120 \pm 13, and 80 ± 9 nm, respectively. In both ELP-(GPO)₆GG and ELP-(GPO)₈GG series, the conjugates formed vesicles with assembly into smaller vesicles observed as the length of the ELP domain increased. Image analysis of the vesicle walls (Fig. 4 and fig. S7) indicates that the thickness of these vesicle walls is 13.7 ± 1.8 nm, 12.5 ± 1.9 nm, 12.9 ± 1.5 nm, 14.4 ± 2.1 nm, and 16.3 ± 2.2 nm, respectively, which is consistent with the estimated R_{σ} of the collapsed ELP domains summed with two triple-helical CLP domains (31), suggesting a bilayer with the CLP domains at both inner and outer surfaces (Fig. 2).

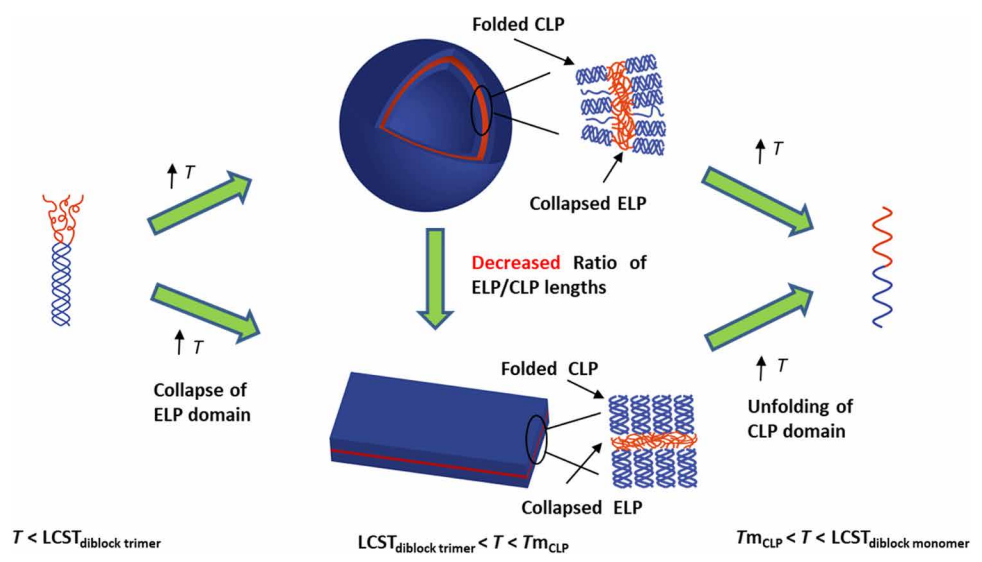


Fig. 2. Proposed assembly/disassembly and bilayer structure of ELP-CLP vesicles and platelets.

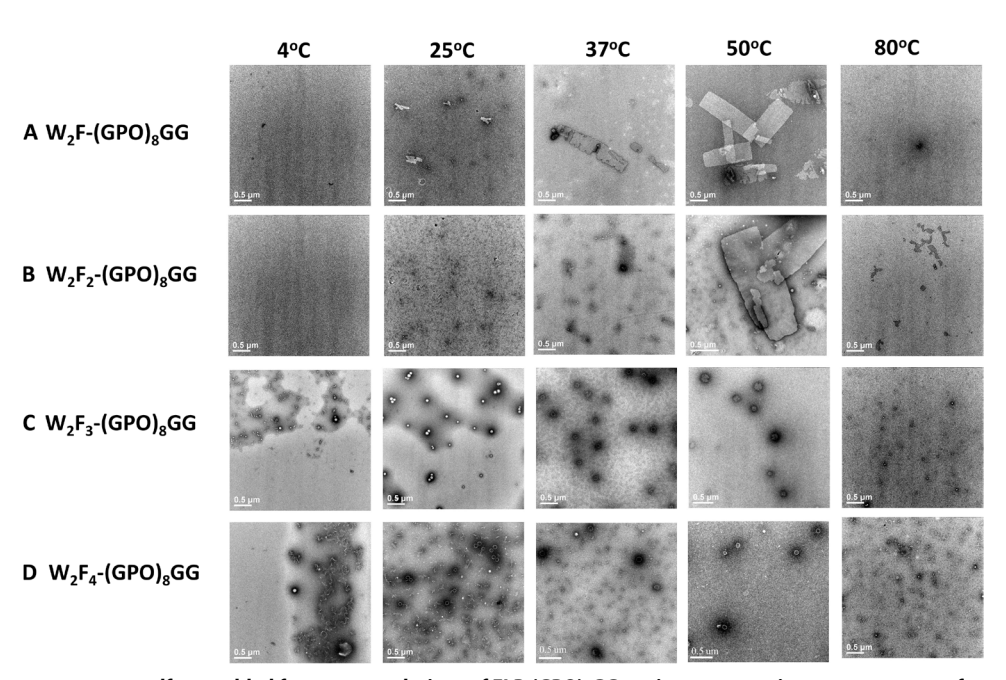


Fig. 3. TEM images of nanostructures self-assembled from water solutions of ELP-(GPO)₈GG conjugates at various temperatures after staining with 2% phosphotungstic acid. (A) W_2F -(GPO)₈GG, (B) W_2F -(GPO)₈GG, (C) W_2F 3-(GPO)₈GG, (D) W_2F 4-(GPO)₈GG. Scale bars, 500 nm.

AFM confirmed the platelet-like structure and thickness of the assemblies of six different ELP-CLP conjugates. The platelets for W_2F -(GPO)₈GG, W_2F_2 -(GPO)₈GG, W_2F_2 -(GPO)₁₀GG, W_2F_3 -(GPO)₁₀GG, and W_2F_4 -(GPO)₁₀GG were demonstrated to have diameters of approximately 500 nm by 1000 nm, 600 nm by 1000 nm, 500 nm by 600 nm, 400 nm by 600 nm, 400 nm by 600 nm, and 400 nm by 600 nm, respectively. Analysis of the each AFM images indicates that the thicknesses of the platelets were 20.4 ± 2.6 , 20.3 ± 2.2 , 21.3 ± 1.7 , 21.9 ± 1.6 , 21.8 ± 1.7 , and 20.6 ± 2.9 nm, respectively (Fig. 5 and figs. S6 and S7), which is perfectly consistent with the expected length of two CLP triple helices combined with the expected size of the collapsed ELP domain, as in our previous conjugates (23), and suggesting an ELP-CLP bilayer structure (Fig. 2).

Because of the relatively low molecular weights of the conjugates, the ratio of the dimensions of the ELP domain to that of the CLP domain conjugates was calculated in contrast to the volume calculations based on homopolymer mass densities; the ratio in lengths was determined by dividing the approximate $R_{\rm g}$ of the collapsed ELP domains (e.g., as in a bad solvent) with the expected length of a folded CLP triple helix (based on known structures of CLPs). As shown in Table 1, these ELP/CLP ratios span values of approximately 0.35 to 0.75 for this set of conjugates. For a set of conjugates with a given CLP domain, platelet-like structures are observed for the conjugates with shorter ELP domains (lower ELP/CLP ratios, below ca. 0.5), while ELP-CLP conjugates with longer ELP domains (higher ELP/CLP ratios) self-assemble into vesicles (summarized in Fig. 6). For

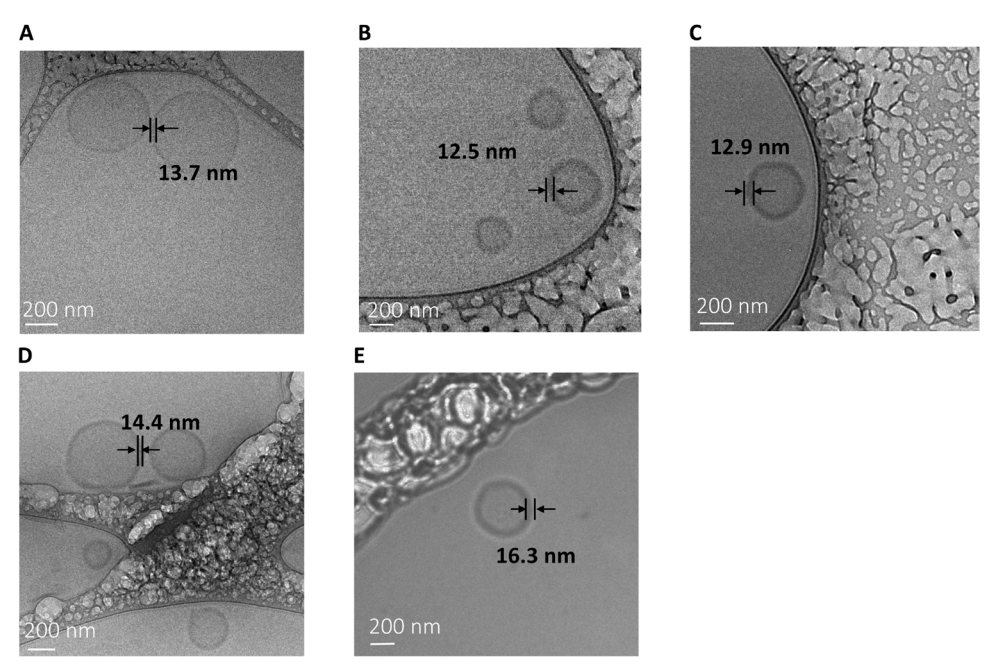


Fig. 4. Cryo-TEM images of nanostructures self-assembled from water solutions at 37°C. (A) W₂F₂-(GPO)₆GG, (B) W₂F₃-(GPO)₆GG, (C) W₂F₄-(GPO)₆GG, (D) W₂F₃-(GPO)₈GG, and (E) W₂F₄-(GPO)₈GG. Scale bars, 200 nm.

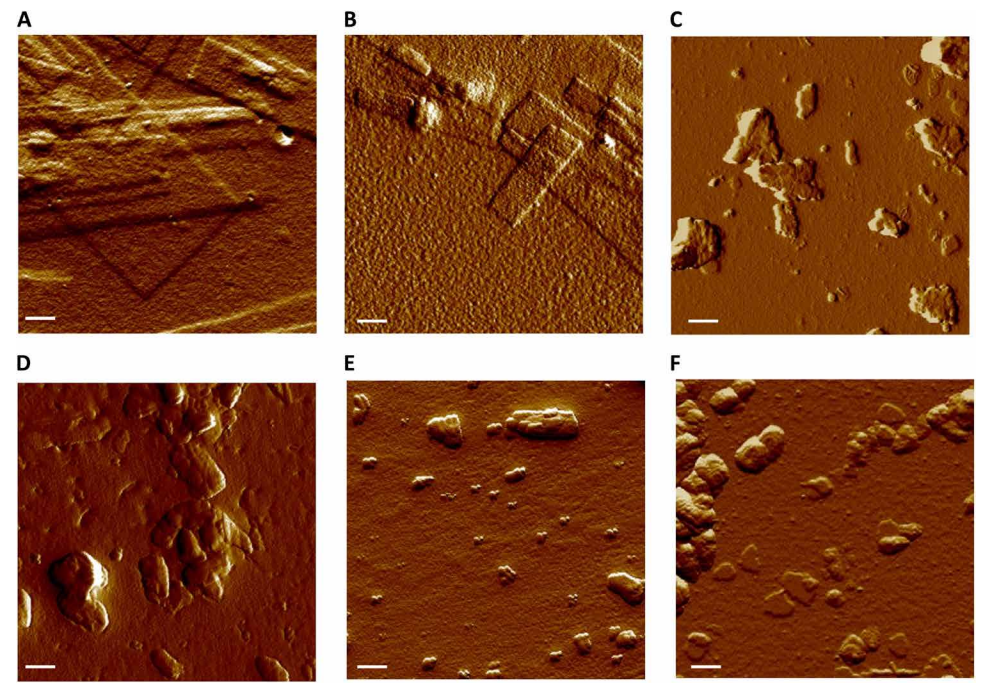


Fig. 5. AFM two-dimensional images of platelet-like assemblies with sample preparation at 45°C. (A) W_2F -GPO₈. (B) W_2F_2 -GPO₈. (C) W_2F -GPO₁₀. (D) W_2F_2 -GPO₁₀. (E) W_2F_3 -GPO₁₀. (F) W_2F_4 -GPO₁₀. Scale bars, 500 nm.

this full set of ELP-CLP conjugates, those with an ELP/CLP ratio lower than 0.51 [value for W_2F_2 -(GPO)₈GG)] self-assemble into platelet-like nanostructures, while those with a ratio greater than 0.54 (value for W_2F_3 -(GPO)₈GG) form nanoscale vesicles. Moreover, vesicle-forming ELP-CLP conjugates with longer ELP domains assemble into vesicles with smaller diameters, indicating that the ratio of ELP-

CLP length directly affects packing, repulsion energy, and ultimately morphology as generally consistent with block copolymer literature (32). The platelet-like ELP-CLP conjugates with shorter CLP domains form slightly larger, more well-defined platelets perhaps due to the difference in the packing of the CLP domain, which has also been observed in some rod-coil copolymer assembly studies (33, 34).

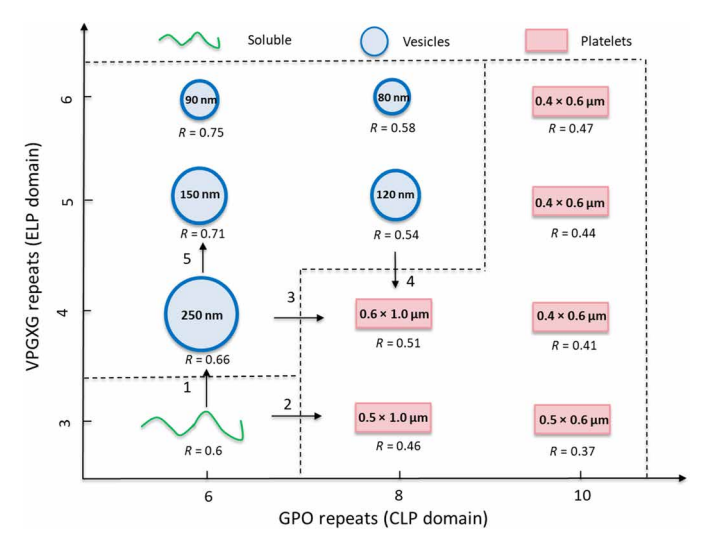


Fig. 6. Diagram indicating transitions in ELP-CLP self-assembly behavior. *R* is the value of ELP/CLP length ratio. The green line indicates the lack of assembly of the conjugate under all conditions tested. The blue circle indicates vesicles with reported diameters as observed via DLS and TEM in the temperature range of assembly, with wall thicknesses determined via cryo-TEM. The red rectangle indicates platelets with reported dimensions as observed via DLS and TEM in the temperature range of assembly, with thicknesses determined via AFM.

DISCUSSION

Amphiphilic copolymers and small molecules self-assemble into various morphologies depending on architectural and chemical features, including block composition, block molecular weight, solvent condition, and the ratio of lengths of the hydrophilic/hydrophobic blocks (32, 35). The change in assembled morphology with variations in the relative volume ratios of the hydrophilic and hydrophobic domains has been widely reported in the literature on synthetic amphiphilic and block copolymers (36-39), and the morphologies of block copolymer nanoparticles can be controlled by a variety of factors including the degree of stretching of the core-forming blocks, the repulsive interactions among chains of the hydrophilic domain, and the interfacial tension between the core and the solvent outside the core (40-42). For example, in polystyrene-b-poly(acrylic acid) (PS-b-PAA) copolymers reported by Eisenberg and coworkers, the degree of stretching and repulsion can be tuned by variations in block length, solvent, and pH to yield various morphologies, with increased repulsion between longer hydrophilic chains driving the morphological transition from vesicle to lamellae (32, 43, 44). In other specific cases, such as poly(4-vinylpyridine) (P4VP) and poly(ε-caprolactone) (PCL) block copolymers (38), when the volume fraction of the hydrophobic P4VP in the block copolymer decreases from 0.95 to 0.33, a morphological transition from vesicles to unclosed bilayer lamellae was observed. In some poly(styrene)block-poly(acrylic acid) (PS-PAA) studies, an increase in hydrophobic block length was also reported to stabilize vesicle structures with increasingly smaller diameters as the length of the hydrophobic segment increased (43, 45). These previous reports are consistent with our observations, in which, for example, the W₂F₄-(GPO)₆GG conjugate (with a longer hydrophobic ELP domain) formed smaller vesicles compared to conjugates with shorter ELP domains [e.g., W₂F₂-(GPO)₆GG, W₂F₃-(GPO)₆GG]. It is likely in these cases that a longer ELP domain occupies a larger volume and would induce

greater interfacial curvature between the ELP and CLP domains so that smaller vesicles with a smaller number of ELP-CLPs would be formed (Fig. 7) (43, 46).

Polypeptide-based amphiphilic molecules can produce sophisticated superstructures as well (47-52). Chilkoti and coworkers (53) have reported recombinant resilin/elastin-like block copolypeptides and studied their morphological transitions between cylindrical micelles and spherical micelles with hydrophilic blocks of various lengths. In their studies, macromolecules with the same ELP_{A/G,80} hydrophilic block exhibited different morphologies depending on the molecular weight (MW) of the hydrophobic resilin-like polypeptide (RLP) block. Increasing the length of the hydrophobic RLP block led to a morphology transition from spherical to cylindrical nanoparticles (53), which is in contrast to our observations in which increasing the length of the hydrophobic domain results in morphologies with greater curvature. This difference in observed behavior may be due to the difference in molecular weights between the two systems and/or due to the rod-coil nature of the ELP(coil)-CLP(rod) conjugates, which likely also supports the ready formation of relatively large nanoscale platelets for conjugates with low ELP/CLP ratios (33, 34); these structures are not observed at all for the resilin/elastin polypeptides.

While many such stimuli-responsive amphiphilic copolymers are widely used as drug carriers (54, 55), dual-responsive copolymer systems are significantly less studied despite their utility. Synthetic polymer-drug conjugates—based largely on polymers such as poly(ethylene glycol), poly(N-isopropylacrylamide), poly(lactic-coglycolic acid), and poly(caprolactone) and sensitive to triggers including pH, temperature, and redox conditions—have shown cleavage of surface groups and/or drugs to control cell trafficking and drug release, self-assembly into polymeric vesicles to control the release of small molecules with cooling (25°C) or heating (60°C), and thiolresponsive delivery of cargo (54-56). Similar studies have been accomplished with peptide-containing molecules. Amphiphilic short peptides and surfactants (C14DMAO) have been used to prepare micellar structures, which are both pH- and metal-ion responsive (56), and pH-sensitive PAMAM-based dendrimers decorated with thermally sensitive elastin-like oligopeptides show LCST transitions that are responsive to physiologically relevant temperatures and pH (57). Photo- and pH-responsive polypeptides with a cell-penetrating peptide sequence (CGRRMKWKK), a photodecomposable group (4,5-dimethoxy-2-nitrobenzyl moieties), and a pH-sensitive inhibitory peptide (EEEERRRR) can enhance the membrane translocation efficiency and transport cargos more selectively and efficiently to tumor cells (58). However, dual thermalresponsive (poly)peptide-based biomaterials have not been reported despite their potential use in ECM targeting of drug delivery vehicles.

In contrast to these previous studies, our reported $[W_2F_{x}-b-(GPO)_y]$ conjugates clearly illustrate important morphological control and triggered responsiveness. The ratio of lengths of the ELP and CLP domains was found to be a critical parameter that can be manipulated to affect the thermoresponsiveness and morphology of resulting ELP-CLP nanostructures. For lower ratios, the assembled conjugates form platelets, with a well-defined transition ratio (ca. 0.50), above which conjugates assemble into vesicles. With increasing ELP/CLP ratio, vesicular nanostructures with significantly smaller diameters were observed, consistent with multiple previous reports of larger copolymer systems. Our report also suggests the impact of the ELP/CLP ratios and assembled morphologies

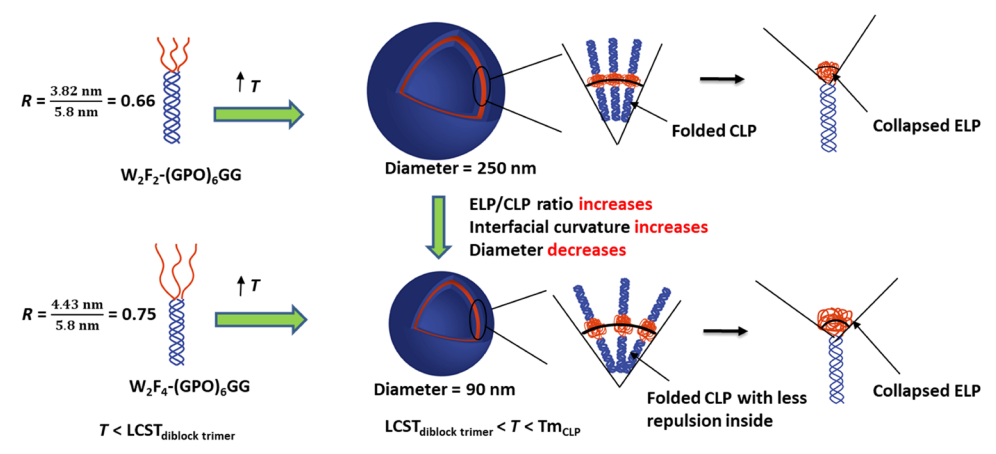


Fig. 7. Proposed morphological transformations for ELP-CLP vesicles.

on the inverse $T_{\rm t}$ and $T_{\rm m}$ of the assembled structures over the full range of experimentally probed temperatures (4° to 80°C), which can be tuned depending on the ELP length, CLP length, and ELP/CLP ratio. These results suggest new opportunities for specific dual temperature-responsive delivery vehicles, which can carry hydrophobic drugs and be used in targeted biological applications. For example, as shown in Table 1, the $T_{\rm m}$ of W₂F₃-(GPO)₆GG is 49°C so that the nanostructures should dissociate and/or more rapidly release drugs at temperatures relevant for hyperthermic drug delivery. Meanwhile, the $T_{\rm t}$ of W₂F₂-(GPO)₈GG is near 43°C, which suggests that with minor modification and/or drug loading, the nanostructures would be suitable for hypothermic targeting applications.

Our studies demonstrate the fine degree of manipulation possible in the transitions and morphologies of dual thermal-responsive conjugates with relatively small changes in conjugate structure. The nanostructures would be useful for the controlled release of drugs by cooling to their $T_{\rm t}$ or heating to their $T_{\rm m}$. The peptidic nature of these conjugates, coupled with their conformational dissimilarity and thermally triggered transitions, offers unique opportunities to finely tune behavior with significantly greater sensitivity than in previous reports. Morphology can be easily tuned with small changes in ELP/CLP and temperature, which promises significant versatility in controlling drug delivery rates and ECM-based targeting of cargo for treatment of diseases characterized by high levels of ECM turnover.

MATERIALS AND METHODS

Materials

Fmoc (9-fluorenyl methoxycarbonyl)–protected amino acids including Fmoc-propargyl glycine, *N*,*N*,*N'*,*N'*-tetramethyl-*O*-(¹H-benzotriazol-1-yl) uronium hexafluorophosphate, and piperidine for SPPS were purchased from AAPPTEC Inc. (Louisville, KY). Rink amide polystyrene resin for SPPS was purchased from CEM Corporation (Matthews, NC). HPLC-grade acetonitrile (ACN) and dimethylformamide (DMF) was purchased from Thermo Fisher Scientific (Fairlawn, NJ). Copper (I) acetate, 4-azidobutanoic acid, trifluoroacetic acid (TFA), triisopropylsilane (TIS), triethylamine, anhydrous DMF, anhydrous dimethyl sulfoxide (DMSO), diisopropylethylamine, ethyl cyanohydroxyiminoacetate (Oxyma), and

diisopropylcarbodiimide (DIC) were purchased from Sigma-Aldrich (St. Louis, MO).

Peptide synthesis

All of the CLPs [with the sequences (GPO)₆GG, (GPO)₈GG, and (GPO)₁₀GG] and tryptophan/phenylalanine-containing elastin-like peptides (W₂F_x) [with sequences VPGWGVPGWGVPGFGG' (W₂F), VPGWGVPGWGVPGFGVPGFGG' (W₂F₂), VPGWGVP-GWGVPGFGVPGFGVPGFGG' (W₂F₃), and VPGWGVPGW-GVPGFGVPGFGVPGFGVPGFGG' (W₂F₄) (G': propargyl glycine)] were synthesized via traditional SPPS methods using a Liberty Blue Automated Microwave Peptide Synthesizer (CEM Corporation, Charlotte, NC). Rink amide polystyrene resin with a loading capacity of 0.19 mmol/g was used for the synthesis. Oxyma was used to activate the amino acids for coupling in the presence of 1 M DIC in DMF. Deprotection of the Fmoc group was conducted using 20% piperidine in DMF. Double coupling of each amino acid at 90°C for 10 min with a 4:1 amino acid/resin ratio was used for the conjugation reactions. For each CLP domain, 4-azidobutanoic acid was then manually attached to the N terminus of CLPs while on resin. The alkyne group from propargyl glycine was introduced to the C terminus of each of the ELP sequences. The cleavage of these peptides from the resin was conducted in 92:4.5:2.5 (v:v:v) TFA:TIS:water for 4 hours. The TFA was evaporated under the flow of nitrogen for 30 min, and the cleaved peptide was precipitated in cold ether. The peptide was then redissolved in water and lyophilized. Crude peptides were purified via reverse-phase HPLC (Waters Inc., Milford, MA) on a Waters XBridge BEH130 Prep C-18 column with an ultraviolet detector at 214 nm and after that were collected and lyophilized. The purity of the peptide (>97%) was confirmed via analytical scale, reverse-phase HPLC (Waters 2996; Symmetry C18, 3.5 µm, 4.6 × 75 mm), and the expected mass of each peptide was confirmed via an ultraperformance liquid chromatographic unit in line with ESI-MS Xevo G2-S QTof (denoted as UPLC-MS) (Waters Corporation, Milford, MA). All samples were dissolved in ACN/water solution at room temperature with concentration of 100 μM. (GPO)₆GG [1844.8 Da (Calc), 1844.5 Da (Exp)], (GPO)₈GG [2380.4 Da (Calc), 2380.2 Da (Exp)], (GPO)₁₀GG [2916.9 Da (Calc), 2916.3 Da (Exp)], W₂F [1566.7 Da (Calc), 1565.8 Da (Exp)], W₂F₂ [2021.2 Da (Calc), 2021.9 Da (Exp)], W₂F₃ [2476.7 Da (Calc), 2476.3 Da (Exp)], and W₂F₄ [2931.3 Da (Calc), 2931.6 Da (Exp)].

ELP-CLP conjugate synthesis

The synthesis of these ELP-CLP conjugates was performed via copper(I)-mediated azide-alkyne cycloaddition reaction. In contrast to our previous report in which click chemistry coupling was conducted in aqueous solution overnight and then ELP-CLP conjugates were purified by dialysis for 7 days (23), in the studies, here, three different reaction protocols were required for the current conjugates owing to the solubility differences of the different CLP domains, and purification of conjugates was conducted via HPLC. For ELP-(GPO)₆GG conjugates, equivalent molar concentrations of CLP (3 μmol) and ELP (3 μmol) were dissolved in 1.0 ml of anhydrous DMF. For ELP-(GPO)₈GG conjugates, the peptides were dissolved at the same concentration and stoichiometry but in 1.0 ml of anhydrous solution of DMF and DMSO (at a volumetric ratio of 7:3 DMF:DMSO). Last, for ELP-(GPO)₁₀GG conjugates, the peptides were dissolved as for the shorter conjugates but in 1.0 ml of deionized (DI) water and anhydrous DMF (at a volumetric ratio of 7:3 DI H₂O:DMF). Then, Cu(I) acetate (0.25 equiv. to alkyne) was added to the solution. The mixture was stirred at 90°C under nitrogen for 4 hours. After the reaction, for ELP-(GPO)₆GG and ELP-(GPO)₈GG conjugates, the resulting peptide conjugate was precipitated into a sevenfold volume of cold diethyl ether and redissolved in 25% ACN/ water solution. The conjugate solution was then purified via HPLC with the gradient set from 25 to 60% ACN over 50 min [for the ELP-(GPO)₆GG and ELP-(GPO)₈GG conjugates]. For ELP-(GPO)₁₀GG conjugates, the conjugate solution was directly injected into HPLC with the gradient set from 30 to 60% ACN over 50 min.

CD spectroscopy

CD spectroscopy (Jasco 810 CD spectropolarimeter, Jasco Inc., Easton, MD, USA) was conducted to characterize the secondary structure of the CLP domain and ELP-CLP conjugates. (GPO)₆GG, (GPO)₈GG, ELP-(GPO)₆GG conjugates, and ELP-(GPO)₈GG conjugates were dissolved at a concentration of 100 µM in DI water at room temperature. (GPO)₁₀GG and ELP-(GPO)₁₀GG conjugates were dissolved at a concentration of 100 µM in 70% H₂O/30% ACN (59) solvent to dissolve the samples at room temperature. Then, these samples were incubated at 4°C overnight before measurement. The CD spectra were recorded using quartz cells with a 0.2-cm optical path length. Full wavelength scans were collected to study the conformation of the triple helix CLP domains at 4°C. The scanning rate was 50 nm/min, with a response time of 4 s. The wavelength scans were obtained from 200 to 250 nm and were recorded every 1 nm. To precisely measure the T_m of the CLP domain, variable temperature experiments were conducted at the maximum wavelength in each ELP-CLP conjugate with a 10°C/hour heating rate from 4° to 80°C.

Dynamic light scattering

Analysis of particle sizes in solution was conducted via DLS on a ZetaSizer Nano Series (Nano ZS, Malvern Instruments, UK) at a scattering angle of 173°, and data fitting using the cumulant method. All samples (1 mg) were dissolved in DI water at a concentration of 1 mg/ml. ELP-CLP conjugates were incubated at 80°C for 30 min so that they melted and formed particles when cooled down at room temperature for overnight before measurement. The inverse $T_{\rm t}$ of the ELP-CLP conjugates were obtained by measuring the average diameters of particles at temperatures from 4° to 80°C at an interval of 3°C. The samples were uniformly opaque with no evidence of

settling during the DLS experiment. Samples were incubated at each temperature for 5 min before data collection. The first derivative of the curve was used to determine the inverse $T_{\rm t}$ for each ELP-CLP conjugate. The reported data represent an average of at least three measurements with the SEM to better represent the spread of the measurements.

Transmission electron microscopy

Samples for TEM were prepared on carbon-coated copper grids (CF300-Cu, Electron Microscopy Sciences Inc.). ELP-CLP conjugates were dissolved in water at concentration of 1 mg/ml [consistent with DLS experiments and to prevent precipitation of the phosphotungstic acid (PTA) stain]. The samples were agitated before sample preparation. The sample solution (5 µl) was drop casted on the grid and blotted after 60 s. For staining, 1% PTA (pH adjusted to 7.0 using 1 M NaOH) as a negative stain was used. The grids, pipette tips, and samples were incubated in an isothermal oven (VWR Signature Forced Air Safety Ovens, VWR Inc.) at desired temperature (4°, 25°, 37°, 50°, and 80°C) for at least 1 hour before sample preparation, which was also conducted in the oven. The PTA solution (3 µl) was drop casted on the grid and blotted after 10 s. The samples were dried in the oven at the desired temperature for 1 hour and then were air-dried for more than 2 hours. TEM images were taken on a 2.1 TEM Tecnai 12 (JEOL USA Inc., Peabody, MA) at an acceleration voltage of 120 keV. Each ELP-CLP conjugate was produced and characterized by three separate times, indicating the repeatable for each ELP-CLP conjugate.

Cryogenic transmission electron microscopy

The thickness of the vesicles prepared by ELP-CLP conjugates was performed in a Talos Cryo-TEM microscope (The Thermo Scientific Talos) operated at 200 kV. Four microliter of the ELP-CLP conjugate solution with concentration (1 mg/ml) in DI water was placed on a copper holey carbon grid (SPI Supplies Inc., West Chester, PA) for 30 s. These samples were blotted twice for 2 s with the blot force of approximately 5 N and then quickly plunged into a liquid ethane reservoir cooled by liquid nitrogen. The vitrified samples were transferred to a Gatan 626 cryo-holder and cryo-transfer stage cooled by liquid nitrogen. During observation of the vitrified samples, the cryo-holder temperature was maintained below -176° C. The images were recorded digitally with a Gatan charge-coupled device camera with 4000×4000 pixel resolution.

Atomic force microscopy

The thickness of the platelets prepared by ELP-CLP conjugates was conducted by AFM (Dimension 3100 V SPM, Bruker). Samples with a concentration of 0.5 mg/ml in DI water were prepared according to the protocol described previously (23). For every sample, ELP-CLP conjugate solution and glass substrates were incubated in a 45°C oven (to exceed the $T_{\rm m}$ of ELP-CLP conjugates) for 1 hour, and 50 μ l of solution was then dropped on the surface of the glass substrate. The AFM sample was dried in the 45°C oven for 2 hour. AFM tips (40 N/m, 320 kHz, Burker) equipped with a 117- μ m by 33- μ m rectangular silicon probe were used to image the platelet-like nanoparticles in the sample.

SUPPLEMENTARY MATERIALS

 $Supplementary\ material\ for\ this\ article\ is\ available\ at\ http://advances.sciencemag.org/cgi/content/full/6/41/eabd3033/DC1$

REFERENCES AND NOTES

- H.-A. Klok, S. Lecommandoux, Supramolecular materials via block copolymer self-assembly. Adv. Mater. 13, 1217–1229 (2001).
- X. Zhao, F. Pan, H. Xu, M. Yaseen, H. Shan, C. A. E. Hauser, S. Zhang, J. R. Lu, Molecular self-assembly and applications of designer peptide amphiphiles. *Chem. Soc. Rev.* 39, 3480–3498 (2010).
- S. Lou, X. Wang, Z. Yu, L. Shi, Peptide tectonics: Encoded structural complementarity dictates programmable self-assembly. Adv. Sci. 6, 1802043 (2019).
- Q. Wang, N. Jiang, B. Fu, F. Huang, J. Liu, Self-assembling peptide-based nanodrug delivery systems. *Biomater. Sci.* 7, 4888–4911 (2019).
- D. Hachim, T. E. Whittaker, H. Kim, M. M. Stevens, Glycosaminoglycan-based biomaterials for growth factor and cytokine delivery: Making the right choices. J. Control. Release 313, 131–147 (2019)
- A. K. Varanko, J. C. Su, A. Chilkoti, Elastin-like polypeptides for biomedical applications. Annu. Rev. Biomed. Eng. 22, 343–369 (2020).
- S. Saha, S. Banskota, S. Roberts, N. Kirmani, A. Chilkoti, Engineering the architecture of elastin-like polypeptides: From unimers to hierarchical self-assembly. Adv. Ther. 3, 1900164 (2020)
- D. E. Meyer, A. Chilkoti, Quantification of the effects of chain length and concentration on the thermal behavior of elastin-like polypeptides. *Biomacromolecules* 5, 846–851 (2004).
- M. Hassan, A. D. Martin, P. Thordarson, Engineering biocompatible scaffolds through the design of elastin-based short peptides. ChemPlusChem 83, 47–52 (2018).
- A. V. Persikov, J. A. M. Ramshaw, B. Brodsky, Prediction of collagen stability from amino acid sequence. J. Biol. Chem. 280, 19343–19349 (2005).
- D. E. Przybyla, J. Chmielewski, Metal-triggered radial self-assembly of collagen peptide fibers. J. Am. Chem. Soc. 130, 12610–12611 (2008).
- A. V. Persikov, J. A. M. Ramshaw, A. Kirkpatrick, B. Brodsky, Amino acid propensities for the collagen triple-helix. *Biochemistry* 39, 14960–14967 (2000).
- L. E. R. O'Leary, J. A. Fallas, E. L. Bakota, M. K. Kang, J. D. Hartgerink, Multi-hierarchical self-assembly of a collagen mimetic peptide from triple helix to nanofibre and hydrogel. Nat. Chem. 3, 821–828 (2011).
- L. E. Bretscher, C. L. Jenkins, K. M. Taylor, M. L. DeRider, R. T. Raines, Conformational stability of collagen relies on a stereoelectronic effect. J. Am. Chem. Soc. 123, 777–778 (2001)
- J. Hwang, M. O. Sullivan, K. L. Kiick, Targeted drug delivery via the use of ECM-mimetic materials. Front. Bioeng. Biotechnol. 8, 69 (2020).
- J. L. Zitnay, Y. Li, Z. Qin, B. H. San, B. Depalle, S. P. Reese, M. J. Buehler, S. M. Yu, J. A. Weiss, Molecular level detection and localization of mechanical damage in collagen enabled by collagen hybridizing peptides. *Nat. Commun.* 8, 14913 (2017).
- J. Hwang, Y. Huang, T. J. Burwell, N. C. Peterson, J. Connor, S. J. Weiss, S. M. Yu, Y. Li, In situ imaging of tissue remodeling with collagen hybridizing peptides. ACS Nano 11, 9825–9835 (2017).
- J. Luo, Y. W. Tong, Self-assembly of collagen-mimetic peptide amphiphiles into biofunctional nanofiber. ACS Nano 5, 7739–7747 (2011).
- T. Luo, K. L. Kiick, Collagen-like peptide bioconjugates. *Bioconjug. Chem.* 28, 816–827 (2017)
- R. Xing, K. Liu, T. Jiao, N. Zhang, K. Ma, R. Zhang, Q. Zou, G. Ma, X. Yan, An injectable self-assembling collagen–gold hybrid hydrogel for combinatorial antitumor photothermal/photodynamic therapy. *Adv. Mater.* 28, 3669–3676 (2016).
- T. Luo, K. L. Kiick, Noncovalent modulation of the inverse temperature transition and self-assembly of elastin-b-collagen-like peptide bioconjugates. J. Am. Chem. Soc. 137, 15362–15365 (2015).
- L. C. Dunshee, M. O. Sullivan, K. L. Kiick, Manipulation of the dually thermoresponsive behavior of peptide-based vesicles through modification of collagen-like peptide domains. *Bioeng. Transl. Med.* 5, e10145 (2020).
- J. Qin, T. Luo, K. L. Kiick, Self-assembly of stable nanoscale platelets from designed elastinlike peptide-collagen-like peptide bioconjugates. *Biomacromolecules* 20, 1514–1521 (2019).
- Y. Yang, D. Nie, Y. Liu, M. Yu, Y. Gan, Advances in particle shape engineering for improved drug delivery. *Drug Discov. Today* 24, 575–583 (2019).
- C. M. Rubert Pérez, N. Stephanopoulos, S. Sur, S. S. Lee, C. Newcomb, S. I. Stupp, The powerful functions of peptide-based bioactive matrices for regenerative medicine. *Annu. Rev. Biomed.* 43, 501–514 (2015).
- N. Habibi, N. Kamaly, A. Memic, H. Shafiee, Self-assembled peptide-based nanostructures: Smart nanomaterials toward targeted drug delivery. *Nano Today* 11, 41–60 (2016).
- A. Prhashanna, P. A. Taylor, J. Qin, K. L. Kiick, A. Jayaraman, Effect of peptide sequence on the LCST-like transition of elastin-like peptides and elastin-like peptide–collagen-like peptide conjugates: Simulations and experiments. *Biomacromolecules* 20, 1178–1189 (2019).
- L. Liang, D. Astruc, The copper(I)-catalyzed alkyne-azide cycloaddition (CuAAC) "click" reaction and its applications. An overview. Coord. Chem. Rev. 255, 2933–2945 (2011).

- H. Nuhn, H. A. Klok, Secondary structure formation and LCST behavior of short elastin-like peptides. Biomacromolecules 9, 2755–2763 (2008).
- A. V. Persikov, J. A. M. Ramshaw, B. Brodsky, Collagen model peptides: Sequence dependence of triple-helix stability. *Biopolymers* 55, 436–450 (2000).
- Y. Zhou, D. Yan, W. Dong, Y. Tian, Temperature-responsive phase transition of polymer vesicles: Real-time morphology observation and molecular mechanism. J. Phys. Chem. B 111, 1262–1270 (2007).
- G. Stirnemann, D. Giganti, J. M. Fernandez, B. J. Berne, Elasticity, structure, and relaxation of extended proteins under force. *Proc. Natl. Acad. Sci. U.S.A.* 110, 3847–3852 (2013).
- L. Zhang, A. Eisenberg, Multiple morphologies and characteristics of "Crew-Cut" micelle-like aggregates of polystyrene-b-poly(acrylic acid) diblock copolymers in aqueous solutions. J. Am. Chem. Soc. 118, 3168–3181 (1996).
- J. J. L. M. Cornelissen, M. Fischer, N. A. J. M. Sommerdijk, R. J. M. Nolte, Helical superstructures from charged poly(styrene)-poly(isocyanodipeptide) block copolymers. *Science* 280, 1427–1430 (1998).
- Y.-b. Lim, K.-S. Moon, M. Lee, Rod-coil block molecules: Their aqueous self-assembly and biomaterials applications. J. Mater. Chem. 18, 2909–2918 (2008).
- E. L. Thomas, D. M. Anderson, C. S. Henkee, D. Hoffman, Periodic area-minimizing surfaces in block copolymers. *Nature* 334, 598–601 (1988).
- Z. Li, M. A. Hillmyer, T. P. Lodge, Morphologies of multicompartment micelles formed by ABC miktoarm star terpolymers. *Langmuir* 22, 9409–9417 (2006).
- I. A. B. Pijpers, L. K. E. A. Abdelmohsen, D. S. Williams, J. C. M. van Hest, Morphology under control: Engineering biodegradable stomatocytes. ACS Macro Lett. 6, 1217–1222 (2017).
- S.-C. Chan, S.-W. Kuo, C.-H. Lu, H.-F. Lee, F.-C. Chang, Syntheses and characterizations
 of the multiple morphologies formed by the self-assembly of the semicrystalline
 P4VP-b-PCL diblock copolymers. *Polymer* 48, 5059–5068 (2007).
- Y. Yu, L. Zhang, A. Eisenberg, Morphogenic effect of solvent on Crew-Cut aggregates of apmphiphilic diblock copolymers. *Macromolecules* 31, 1144–1154 (1998).
- L. Zhang, A. Eisenberg, Formation of crew-cut aggregates of various morphologies from amphiphilic block copolymers in solution. *Polym. Adv. Technol.* 9, 677–699 (1998).
- B. M. Discher, H. Bermudez, D. A. Hammer, D. E. Discher, Y.-Y. Won, F. S. Bates, Cross-linked polymersome membranes: Vesicles with broadly adjustable properties. J. Phys. Chem. B 106, 2848–2854 (2002).
- H. Bermudez, A. K. Brannan, D. A. Hammer, F. S. Bates, D. E. Discher, Molecular weight dependence of polymersome membrane structure, elasticity, and stability. *Macromolecules* 35, 8203–8208 (2002).
- T. Azzam, A. Eisenberg, Control of vesicular morphologies through hydrophobic block length. Angew. Chem. Int. Ed. Engl. 45, 7443–7447 (2006).
- L. Luo, A. Eisenberg, Thermodynamic stabilization mechanism of block copolymer vesicles. J. Am. Chem. Soc. 123, 1012–1013 (2001).
- 46. P. Lim Soo, A. Eisenberg, Preparation of block copolymer vesicles in solution. *J Polym Sci B*
- H. Schlaad, L. You, R. Sigel, B. Smarsly, M. Heydenreich, A. Mantion, A. Mašić, Glycopolymer vesicles with an asymmetric membrane. *ChemComm* 2009, 1478–1480 (2009).
- Z. Li, T. J. Deming, Tunable hydrogel morphology via self-assembly of amphiphilic pentablock copolypeptides. Soft Matter 6, 2546–2551 (2010).
- Y. Lu, A. A. Aimetti, R. Langer, Z. Gu, Bioresponsive materials. Nat. Rev. Mater. 2, 16075 (2016).
- D. Roy, W. L. A. Brooks, B. S. Sumerlin, New directions in thermoresponsive polymers. Chem. Soc. Rev. 42, 7214–7243 (2013).
- A. Carlsen, S. Lecommandoux, Self-assembly of polypeptide-based block copolymer amphiphiles. Curr. Opin. Colloid Interface Sci. 14, 329–339 (2009).
- L. Zhao, N. Li, K. Wang, C. Shi, L. Zhang, Y. Luan, A review of polypeptide-based polymersomes. *Biomaterials* 35, 1284–1301 (2014).
- I. Weitzhandler, M. Dzuricky, I. Hoffmann, F. Garcia Quiroz, M. Gradzielski, A. Chilkoti, Micellar self-assembly of recombinant resilin–/elastin-like block copolypeptides. Biomacromolecules 18, 2419–2426 (2017).
- L. Zhang, R. Guo, M. Yang, X. Jiang, B. Liu, Thermo and pH dual-responsive nanoparticles for anti-cancer drug delivery. Adv. Mater. 19, 2988–2992 (2007).
- J.-Z. Du, X.-J. Du, C.-Q. Mao, J. Wang, Tailor-made dual pH-sensitive polymer–doxorubicin nanoparticles for efficient anticancer drug delivery. J. Am. Chem. Soc. 133, 17560–17563 (2011).
- D. Wang, Y. Sun, M. Cao, J. Wang, J. Hao, Amphiphilic short peptide modulated wormlike micelle formation with pH and metal ion dual-responsive properties. RSC Adv. 5, 95604–95612 (2015).
- T. Koga, M. limura, N. Higashi, Novel peptide-shelled dendrimer with dramatically changeable thermo-responsive character. *Macromol. Biosci.* 12, 1043–1047 (2012).
- Y. Yang, X. Xie, Y. Yang, Z. Li, F. Yu, W. Gong, Y. Li, H. Zhang, Z. Wang, X. Mei, Polymer nanoparticles modified with photo- and pH-dual-responsive polypeptides for enhanced and targeted cancer therapy. *Mol. Pharm.* 13, 1508–1519 (2016).

SCIENCE ADVANCES | RESEARCH ARTICLE

 K. Kandori, Y. Uoya, T. Ishikawa, Effects of acetonitrile on adsorption behavior of bovine serum albumin onto synthetic calcium hydroxyapatite particles. *J. Colloid Interface Sci.* 252, 269–275 (2002).

Acknowledgments

Funding: This work was funded in part by the National Institutes of Health (R21 AR069778A, 1 P30 GM110758, and both 1 P30 GM103519 and 1 P20 GM104316 for instrument resources) and in part by the National Science Foundation (CBET 1703402). The contents of this manuscript do not necessarily reflect the views of the funding agencies. **Author contributions:** The conjugate design, experimental protocols, and data analysis were conducted by J.Q. and K.L.K. The experimental work such as conjugate synthesis, purification, and characterization, CD measurements, DLS measurements, TEM characterization, and AFM analysis were are all conducted by J.Q. Cryo-TEM measurements were performed by J.D.S. All authors discussed the results and contributed to the manuscript. J.Q. and K.L.K wrote the

original draft and handled the editing. **Competing interests:** K.L.K. is an inventor on a patent related to this work filed by the University of Delaware (no. 10,639,371, filed 29 July 2016, published 5 May 2020). The authors declare that they have no other competing interests. **Data and materials availability:** All data needed to evaluate the conclusions in the paper are presented in the paper and/or the Supplementary Materials. Additional data related to this paper may be requested from the authors.

Submitted 12 June 2020 Accepted 26 August 2020 Published 7 October 2020 10.1126/sciadv.abd3033

Citation: J. Qin, J. D. Sloppy, K. L. Kiick, Fine structural tuning of the assembly of ECM peptide conjugates via slight sequence modifications. *Sci. Adv.* **6**, eabd3033 (2020).



Fine structural tuning of the assembly of ECM peptide conjugates via slight sequence modifications

Jingya Qin, Jennifer D. Sloppy and Kristi L. Kiick

Sci Adv **6** (41), eabd3033. DOI: 10.1126/sciadv.abd3033

ARTICLE TOOLS http://advances.sciencemag.org/content/6/41/eabd3033

SUPPLEMENTARY http://advances.sciencemag.org/content/suppl/2020/10/05/6.41.eabd3033.DC1 MATERIALS

REFERENCES This article cites 59 articles, 3 of which you can access for free

http://advances.sciencemag.org/content/6/41/eabd3033#BIBL

PERMISSIONS http://www.sciencemag.org/help/reprints-and-permissions

Use of this article is subject to the Terms of Service